QUANTITATIVE MEASUREMENT OF DELAMINATION GROWTH IN COMPOSITE LAMINATES WITH SMALL-DIAMETER FIBER BRAGG GRATING SENSORS

Nobuo Takeda, Yoji Okabe and Shin-ichi Takeda

Department of Advanced Energy, Graduate School of Frontier Sciences, The University of Tokyo,
5-1-5 Kashiwanoha, Kashiwa-shi, Chiba 277-8561, Japan

ABSTRACT

Small-diameter fiber Bragg grating (FBG) sensors, whose outside diameter was 52μm, were applied to the detection of delaminations in CFRP laminates. Reflection spectra from the embedded FBG sensors deformed because of the change in the strain distribution due to a delamination. Since these deformations of the spectra could be reproduced by theoretical calculations, it was found that the small-diameter FBG sensors could detect the occurrence of the delamination caused by a cyclic loading or a low-velocity impact and evaluate the delamination length quantitatively. Furthermore, this technique was applied to the detection of debonding of a CFRP repair patch from an aluminium substrate.

1. INTRODUCTION

FBG sensors are very sensitive to non-uniform strain distribution along the entire length of the grating [1]. The strain distribution deforms the reflection spectrum from the FBG sensors. Taking advantage of the sensitivity, the authors applied FBG sensors for detecting transverse cracks that caused non-uniform strain distribution in CFRP laminates [2]. However, the cladding of common optical fibers is 125μm in diameter, which is almost the same as the normal thickness of one ply in CFRP laminates. Thus, when the normal FBG sensors are embedded into CFRP composites, there is a possibility that the optical fibers might deteriorate the mechanical properties of the laminates. In order to prevent the deterioration, small-diameter FBG sensors have recently been developed by the authors and Hitachi Cable Ltd. [3]. The outside diameter of the polyimide coating is 52μm, and the cladding is 40μm in diameter. The small-diameter FBG sensors could detect transverse cracks in CFRP laminates sensitively [4]. In this research, the sensors were applied to detect edge delaminations in the laminates under cyclic loading and delaminations caused by low-velocity impact. Furthermore, this technique was applied to the detection of debonding of a CFRP repair patch from an aluminum substrate.

2. DETECTION OF EDGE DELAMINATION UNDER CYCLIC LOADING

2.1 Experimental Procedure

Bragg gratings were fabricated in small-diameter optical fibers. The outside diameters of the polyimide coating, the cladding, and the core are 52μm, 40μm, and 6.5μm, respectively. The grating length is 10mm, and the grating period is about 0.5μm. The FBG sensor was embedded in a 90^o ply in contact with a $0^o/90^o$ interface of a CFRP T700S/2500 quasi-isotropic laminate (Toray Industries, Inc.) whose laminate configuration was [+45/-45/0/90]s [5]. The FBG sensor of 10mm gauge length was located at the position of 0 to 10mm from the center of the specimen as shown in Fig. 1.

Cyclic tensile load was applied to the specimen from 0 to 440MPa at room temperature. The frequency of the loading cycle was 5Hz. After the cyclic loading was stopped at the pre-determined numbers of cycles, the reflection spectra from the FBG sensor were measured at both stress levels of 0MPa and 220MPa using an ASE light source unit (Ando Electric Co., Ltd., AQ4310(155)) and an optical spectrum analyzer (Ando Electric Co., Ltd., AQ6317).

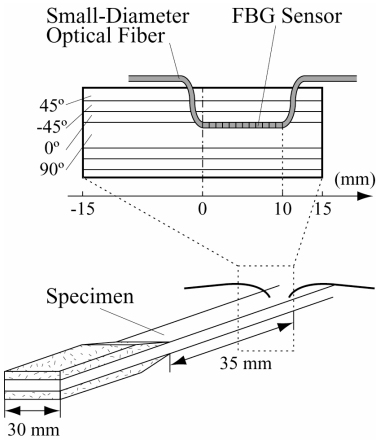

Fig. 1 Embedding of a small-diameter FBG sensor into a CFRP quasi-isotropic laminate.

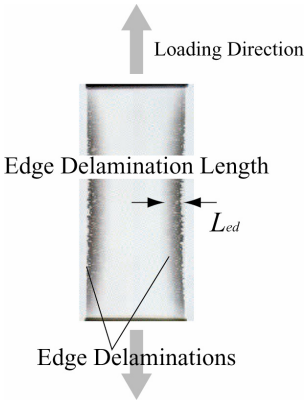

Fig. 2 Soft X-ray photograph of the specimen and definition of the edge delamination length L_{ed}.

2.2 Experimental Results

Fig. 2 shows a soft X-ray photograph of the specimen in which the edge delaminations occurred after loading cycles of 100,000. In this study, an edge delamination length L_{ed} was defined as the length of a delamination in the width direction and determined from the X-ray photograph. The edge delamination grew with an increase in number of cycles as summarized in Table 1. The spectra measured at each step are shown in Fig. 3. The intensity of the spectrum was normalized by the highest component. Before the cyclic load was applied to the specimen (step 0), the spectrum had one peak. After the occurrence of the delamination, though the drastic change in the form of the spectrum measured after unloading was not observed in all steps, the spectrum measured at the stress level of 220MPa changed its form with an increase in the delamination length. When the tip of the edge delamination reached the position of the FBG sensor (step3), the spectrum was divided into two peaks. As the delamination length increased (from step 3 to step 4), the intensity of the longer wavelength peak increased relatively.

Table 1 Edge delamination length at various number of cycles.

	Number of cycles ($\times 10^3$)	Edge delamination length (mm)
Step 0	0	0
Step 1	1	2.8
Step 2	20	5.2
Step 3	100	7.4
Step 4	1000	9.0

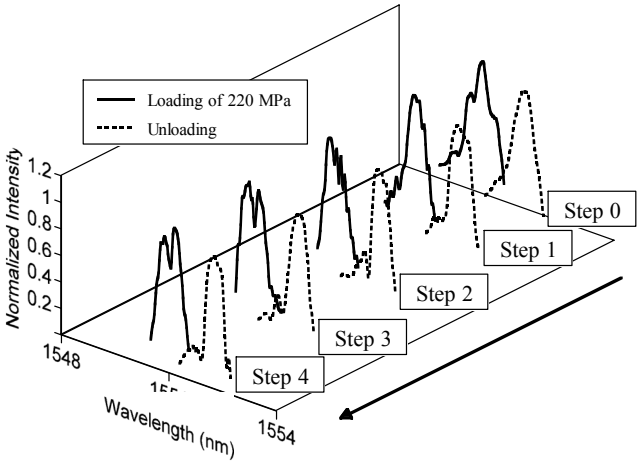

Fig. 3 Measured reflection spectra.

2.3 Analysis

For confirmation of the measured results, the reflection spectrum was simulated by theoretical analysis. First, the axial strain distribution in the small-diameter optical fiber embedded in a laminate was calculated by 3-D FEM analysis with ABAQUS code. The FEM model was just

1/8 part of the test specimen and consisted of a glass optical fiber, a polyimide coating and a CFRP laminate. The edge delamination at $0^o/90^o$ interface or in the middle of the 90^o ply was assumed as quadrilateral shape, and the thermal residual stress was introduced by cooling from the manufacturing temperature of 130^oC to the room temperature of 25^oC. Next, the distributions of the grating period and the average refractive index of the FBG were calculated from the axial strain distribution [6]. Then the reflection spectrum was simulated from the distributions by solving couple mode equations with transfer matrix method [7].

Figure 4 shows the calculated spectra after unloading. When the edge delamination is assumed to exist in the middle of the 90^o ply, the spectrum does not change. This is because the delamination in that position hardly disturbs the distribution of the longitudinal thermal residual strain. On the other hand, when the edge delamination appears at the $0^o/90^o$ interface and the L_{ed} is over 5mm, the spectrum has two peaks. In this case, the compression thermal residual strain is released by the delamination, so that the axial strain distribution consists of two levels of uniform strain. The larger strain level at the delaminated area corresponds to the longer wavelength peak in the spectrum, and the smaller strain level at the bonded area corresponds to the shorter wavelength peak. Thus, the intensity of the longer wavelength peak increases with an increase in the L_{ed}.

Figure 5 shows the calculated spectra under loading of 220MPa. When the laminate is strained longitudinally, the bonded area is compressed by Poisson's effect, and the difference of the strain level between the delaminated and the bonded areas increases. Hence, the distance between the two peaks in the spectrum increases, and the spectrum for the case of the $0^o/90^o$ interface delamination also has two peaks. These results indicate that the edge delamination will be easily detected by applying a tensile loading.

Compared with these calculated spectra in Figs. 4 and 5, the measured spectra in Fig. 3 show the same tendency of the deformation as the case of the 90^o intralaminar delamination. When a cross section of the specimen after the cyclic loading was observed, the edge delamination existed in the 90^o ply. Thus, these calculation results are consistent with the experimental results. From these results, the intensities of the two peaks in the spectrum were found to correspond to the lengths of delaminated and bonded areas. Thus, the intensity ratio of the two peaks I_L/I_S is defined as an indicator to evaluate the delamination size. Here, I_L and I_S are the intensities of the longer and shorter wavelength peaks, respectively. Figure 6 shows the logarithmic plot of the intensity ratio against L_{ed}. Both the experimental and calculated results have the same tendency that the I_L/I_S increases with an increase in L_{ed}. Thus the delamination

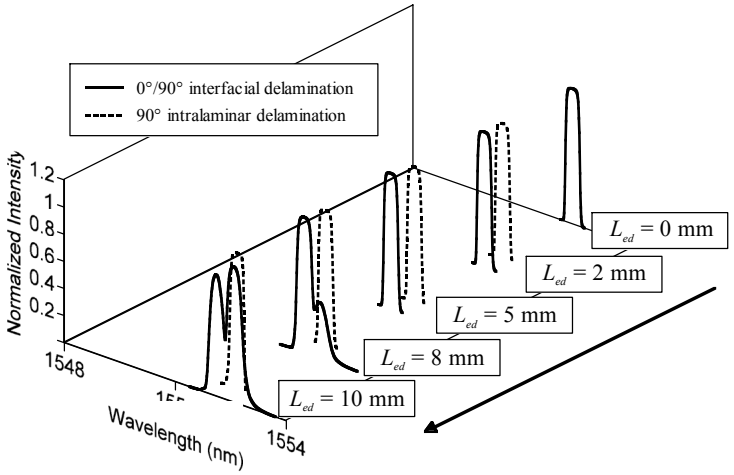

Fig. 4 Calculated spectra after unloading.

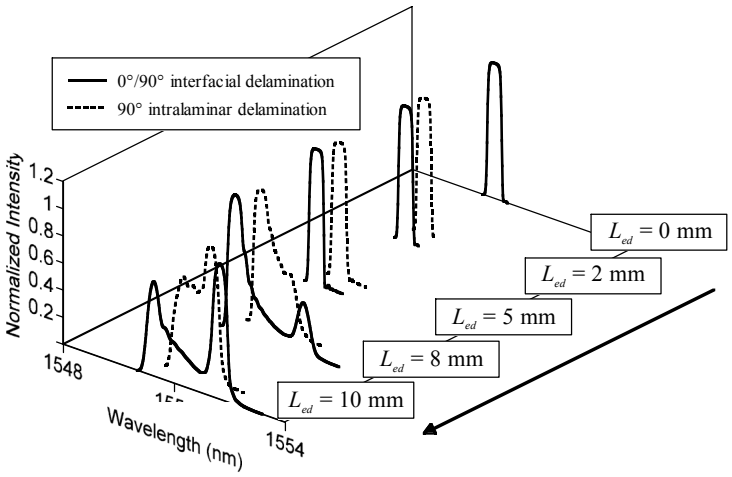

Fig. 5 Calculated spectra under loading of 220MPa.

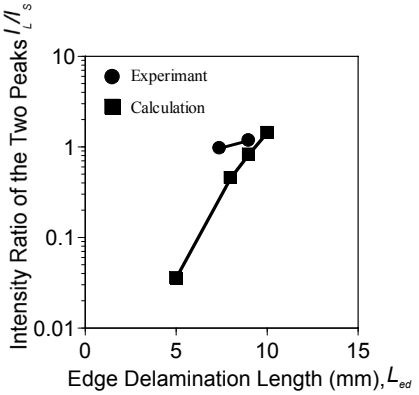

Fig. 6 Intensity ratios of the two peaks against L_{ed}.

length L_{ed} can be estimated from the intensity ratio I_L/I_S. Moreover, as shown in Fig. 5, the distance between the two peaks in the spectrum can indicate whether the edge delamination grew at the $0^o/90^o$ interface or in the middle of the 90^o ply.

3. DETECTION OF DELAMINATION INDUCED BY LOW-VELOCITY IMPACT

Low-velocity impact easily induces delaminations and matrix cracks in CFRP laminates, which are barely visible from the outer surface. For practical use of the CFRP laminates, it is important to monitor the damage state in real time. In this section, the above detection technique is applied to the delamination induced by low-velocity impact [8].

3.1 Experimental Procedure

The specimen was CFRP laminates T700S/2500, and the laminate configuration was cross-ply $[0_4/90_4/0_4]$. The dimensions of the test specimen were $100 \times 100 \times 1.5$ mm^3. The impact loading was applied to the specimen with a drop-weight impact tester (Instron Corporation, Dynatup Mini-Tower). The applied impact energies were 1.0J, 1.2J, 2.0J, and 3.0J. After the impact test, interlaminar delaminations were observed by an ultrasonic C-scan. The schematic of the damages in the laminate are illustrated in Fig. 7. Furthermore, cross-sectional micrographs at P, Q, and R planes in Fig. 7 are shown in Fig. 8. Typical damages in the laminate were two peanut-shape delaminations at upper and lower $0^o/90^o$ interfaces, shear cracks in 90^o ply, and a bending crack in lower 0^o ply. The small-diameter FBG sensor was embedded into 90^o ply in contact with the lower $0^o/90^o$ interface as shown in Fig. 7 in order to detect the delamination at the lower interface. The reflection spectrum from the embedded FBG was measured using the optical spectrum analyzer after the impact test.

3.2 Experimental Results

Figure 9 shows photographs of the lower $0^o/90^o$ interfacial delamination observed by ultrasonic C-scan. The size of the delamination increased with an increase in the impact energy level. A bending crack also appeared in all the pictures. The reflection spectra measured before and after the impact tests are shown in Fig. 10. These were normalized by the intensity of the highest component. When the impact energy was 1.0J, the delamination

did not reach to the FBG sensor and the bending crack passed under the sensor. In this case, the reflection spectrum was deformed drastically. As the impact energy increased, the delamination area passing through the FBG sensor increased and the longer wavelength peak in the spectrum became larger. When the delamination area covered the whole FBG sensor at the impact energy of 3.0J, the spectrum shifted to the longer wavelength position keeping its shape.

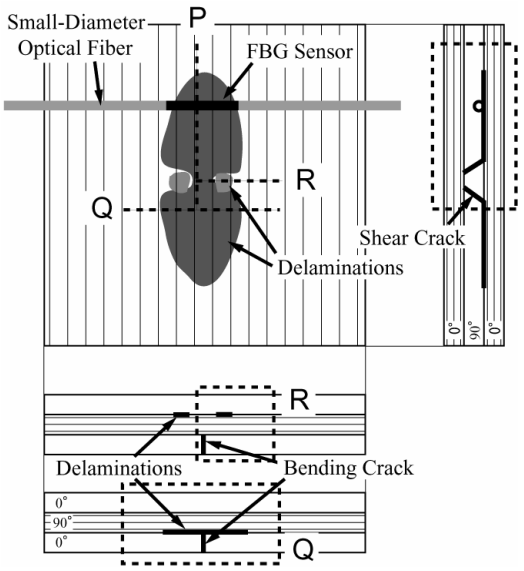

Fig. 7 Schematic of the specimen configurations and typical damages in the cross-ply laminate.

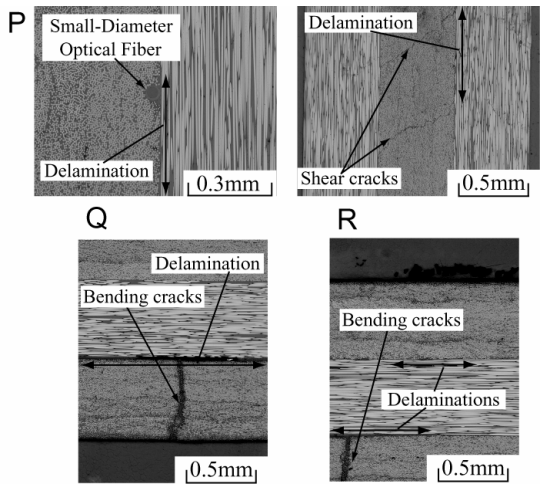

Fig. 8 Cross-sectional micrographs of the damaged laminates.

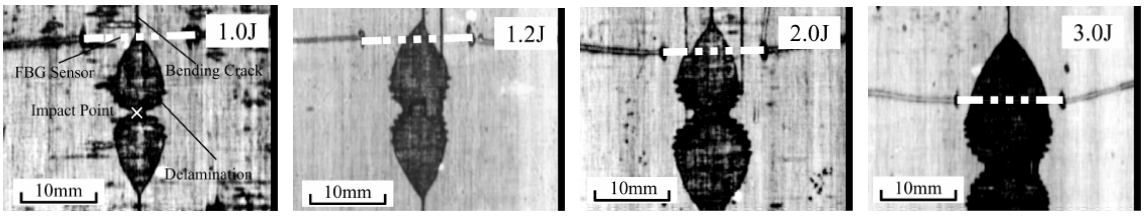

Fig. 9 Photographs of the lower $0^o/90^o$ interfacial delamination observed by ultrasonic C-scan.

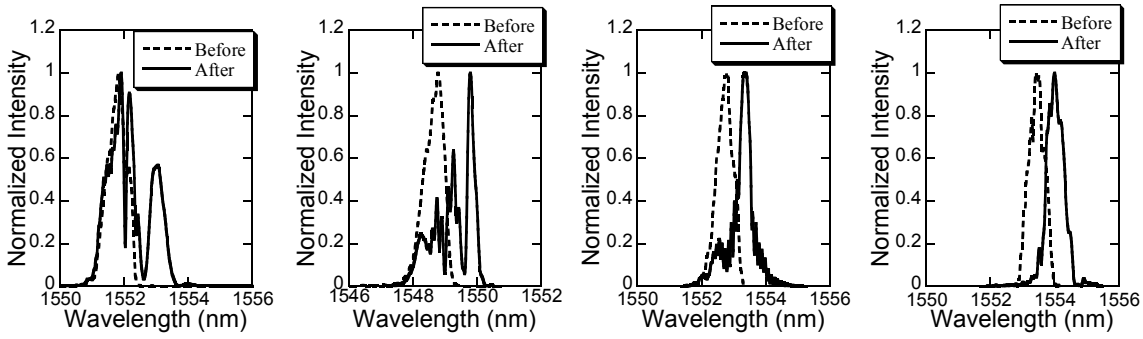

Fig. 10 Measured reflection spectra.

3.3 Analysis

Also, these experimental results were confirmed by theoretical calculations in the same way as the analysis procedure described in the above chapter. The 1/4 part of the specimen was modeled by using 3D finite elements. In this model, the lower $0^o/90^o$ interface delamination, shear cracks in 90^o ply and a bending crack in the lower 0^o ply were introduced. From the analysis, the strain distribution at 27μm above from the lower $0^o/90^o$ interface, where the center of the optical fiber was located, was obtained. Then, the reflection spectrum was simulated using the axial strain distribution. The calculated spectra are shown in Fig. 11. These shapes of the spectra well reproduced those of the measured ones in Fig. 10. This agreement indicates that the deformation of the spectrum at the impact energy of 1.0J is caused by the strain concentration around the tip of the bending crack. The large peak at the longer wavelength in the spectra at 1.2J and 2.0J corresponds to the strain at the delaminated area, and the some components at the shorter wavelength are caused by the change in the strain distribution around the delamination tip. The spectrum at 3.0J is not deformed, because the whole gauge length of the FBG is covered with the delamination and is under uniform strain. The center wavelength shift of the spectrum by the impact of 3.0J corresponds to the strain difference between the bonded and the delaminated areas. From these results, it was found that the small-diameter FBG sensor could detect the delamination induced by low-velocity impacts.

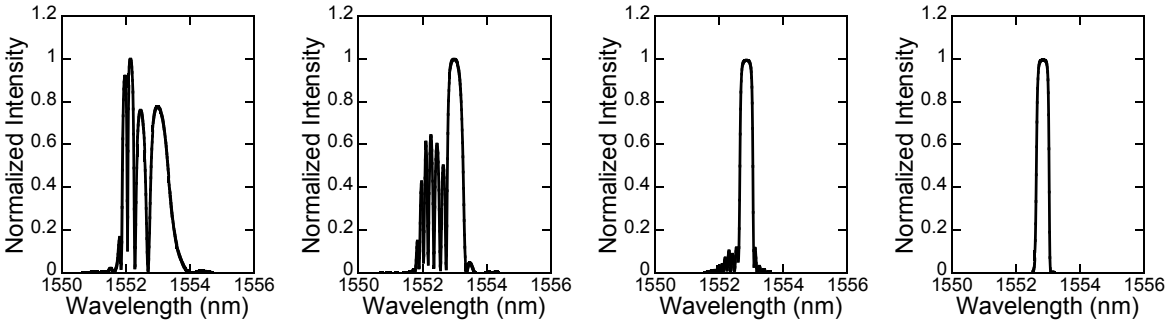

Fig. 11 Calculated reflection spectra, which correspond to the measured spectra in Fig. 10.

4. DEBONDING DETECTION OF COMPOSITE REPAIR PATCH

In recent years airworthiness of aging aircrafts is required to be extended, so that bonded composite patches are used for repairing fatigue cracks. However, the repair deteriorates when the patch is debonded. Thus, the authors attempted to detect the debonding of a composite repair patch using the small-diameter FBG sensor as a further application of the delamination detection technique [9].

4.1 Experimental Procedure

The patches were CFRP unidirectional laminates T800H/3631 $[0]_4$ and were glued on both sides of an aluminum plate Al-5052 using adhesive films AF-163-2K as shown in Fig. 12. Before embedding of the small-diameter FBG sensor, cyclic tensile load was applied to the aluminum plate to which the patches adhered without the FBG from 0 to 200MPa at 5Hz, and the debonding of the patch from the plate was observed. As a result, it was found that delaminations appeared between the adhesive and the aluminum plate from the ends of the adhesive layer and progressed along the loading direction as shown in Fig. 13. Then, in order to determine the embedment position of the FBG sensor in the thickness direction, the spectrum from the FBG was simulated using 3-D FEM analysis considering the observed

delamination progress. The calculated results indicated that the form of the spectrum became complex as the embedment position approached to the interface between the adhesive and the aluminum. Thus, the small-diameter FBG sensor was decided to be embedded away from the delamination and in contact with the CFRP patch as shown in Fig. 13. One end of the FBG sensor, whose grating length was 10mm, was located at 5mm away from the end of the adhesive layer. Then the cyclic tensile loading was applied to the repaired aluminum plate with the FBG sensor. After the loading was stopped at the pre-determined numbers of cycles, the reflection spectrum was measured at the stress level of 200MPa.

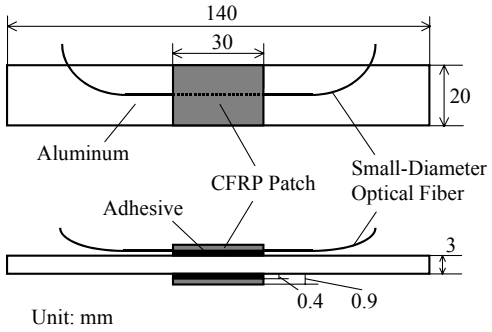

Fig. 12 Aluminum plate repaired with CFRP patches.

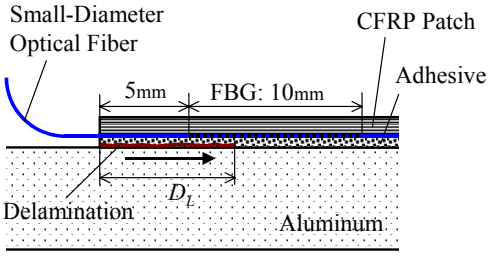

Fig. 13 Schematic of the delamination progress and the embedment position of the small-diameter FBG sensor.

4.2 Experimental Results

Figure 14 shows the reflection spectra measured at various delamination lengths. Here the delamination length D_L was defined as the length of the delamination in the loading direction. With an increase in the delamination length, another peak appeared at shorter wavelength, and the intensity of the shorter wavelength peak increased relatively.

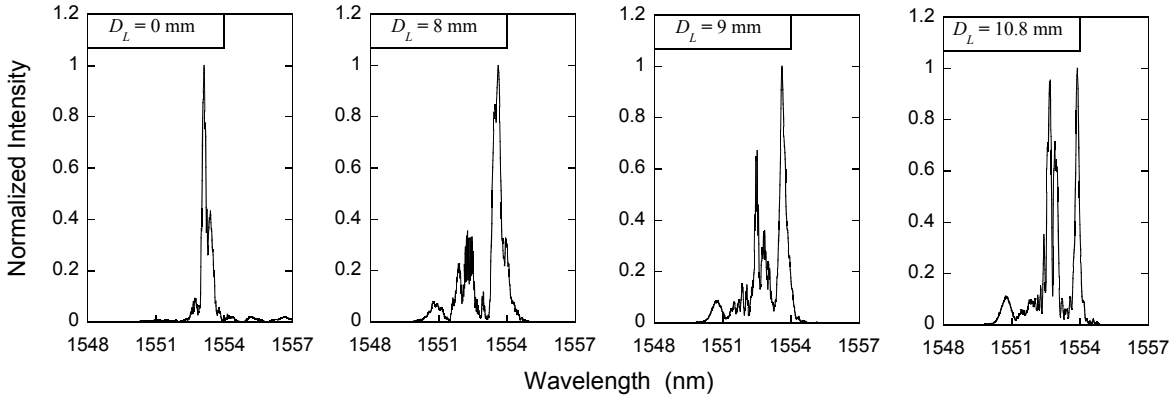

Fig. 14 Reflection spectra from the small-diameter FBG sensor embedded in the adhesive layer, measured at various delamination lengths D_L.

4.3 Analysis

These experimental results were also simulated theoretically in the same way. The calculated spectra are shown in Fig. 15. The change in the spectra shows the same tendency with that in the measured spectra. In this case, the tensile strain in the adhesive layer due to the tensile loading applied to the aluminum plate is released by the delamination, so that the shorter

wavelength peak grows as the delamination length increases. Thus, the intensity ratio of the two peaks I_S/I_L was plotted in Fig. 16. Since the both intensity ratios obtained by the experiment and the simulation increases with an increase in the delamination length, the debonding of the CFRP patch can be evaluated quantitatively using the small-diameter FBG sensor.

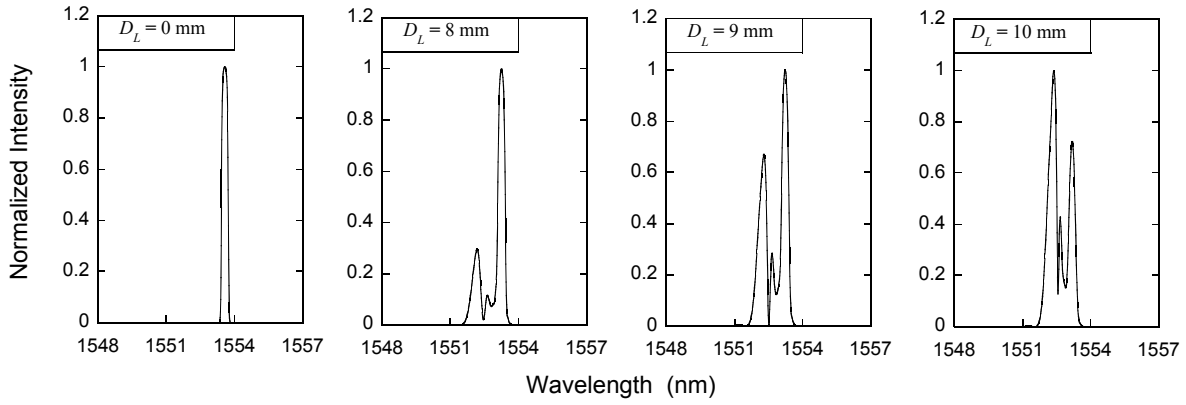

Fig. 15 Reflection spectra calculated at various delamination lengths D_L.

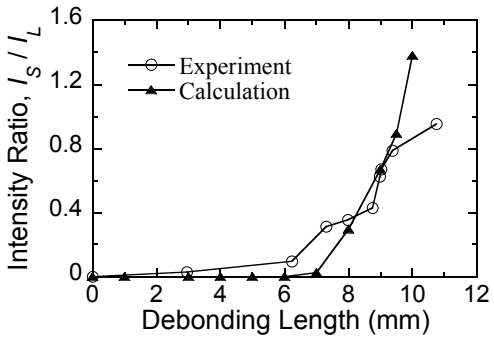

Fig. 16 Intensity ratios of the two peaks I_S/I_L against the delamination length.

5. CONCLUSIONS

In this research, newly developed small-diameter FBG sensors, whose outside diameter was 52μm, were applied to detect delaminations in CFRP laminates. First, for the detection of the edge delamination, the FBG sensor was embedded into the 90° ply of a quasi-isotropic laminate $[+45/-45/0/90]_s$. As the edge delamination length increased under cyclic loading, two peaks appeared in the reflection spectrum, and those intensities changed depending on the delamination length. This deformation of the spectrum could be reproduced by theoretical calculations. Hence, it was found that the delamination length could be predicted using the intensity ratio of the two peaks, and the distance between the two peaks indicated whether the delamination grew at the 0°/90° interface or in the middle of the 90° ply.

Secondly, this technique was applied to the detection of the delamination induced by low-velocity impacts. The small-diameter FBG sensor was embedded into the 90° ply of a cross-ply laminate $[0_4/90_4/0_4]$, and a low-velocity impact was applied to the laminate at four levels of impact energies: 1.0J, 1.2J, 2.0J, and 3.0J. As a result, the reflection spectrum was deformed depending on the delamination size, and this change agreed with theoretical

calculations. Thus, the small-diameter FBG sensor could also detect the delamination induced by low-velocity impacts.

Furthermore, it was attempted to detect the debonding of a composite repair patch as a further application of the delamination detection technique. The small-diameter FBG sensor was embedded into the adhesive layer between the CFRP patch and the aluminum plate. The experimental result and the calculation result showed that the delamination length between the adhesive layer and the aluminum plate could be evaluated from the intensity ratio of the two peaks in the reflection spectra.

References

1. **Huang, S.**, **Ohn, M.M.**, **LeBlanc, M.** and **Measures, R.M.**, "Continuous arbitrary strain profile measurements with fiber Bragg gratings", *Smart Mater. Struct.*, **7**/2 (1998), 248-256.
2. **Okabe, Y.**, **Yashiro, S.**, **Kosaka, T.** and **Takeda, N.**, "Detection of transverse cracks in CFRP composites using embedded fiber Bragg grating sensors", *Smart Mater. Struct.*, **9**/6 (2000), 832-838.
3. **Satori, K.**, **Fukuchi, K.**, **Kurosawa, Y.**, **Hongo, A.** and **Takeda, N.**, "Polyimide-coated small-diameter optical fiber sensors for embedding in composite laminate structures", *Smart Structures and Materials 2001: Sensory Phenomena and Measurement Instrumentation for Smart Structures and Materials, Udd, E. and Inaudi, D. eds., Proc. SPIE vol. 4328* (2001), 285-294.
4. **Okabe, Y.**, **Mizutani, T.**, **Yashiro, S.** and **Takeda, N.**, "Detection of microscopic damages in composite laminates with embedded small-diameter fiber Bragg grating sensors", *Compos. Sci. Technol.*, **62**/7-8 (2002), 951-958.
5. **Takeda, S.**, **Okabe, Y.**, **Yamamoto, T.** and **Takeda, N.**, "Detection of edge delamination in CFRP laminates under cyclic loading using small-diameter FBG sensors", *Compos. Sci. Technol.*, **63**/13 (2003), 1885-1894.
6. **Van Steenkiste, R.J.** and **Springer, G.S.**, *Strain and Temperature Measurement with Fiber Optic Sensors*, Technomic, Lancaster (1997).
7. **Kashyap, R.**, *Fiber Bragg Gratings*, Academic Press, San Diego (1999).
8. **Minakuchi, S.**, **Takeda, S.**, **Okabe, Y.** and **Takeda, N.**, "Detection of impact damages in CFRP cross-ply laminates using small-diameter FBG sensors", *Proc. 8th Japan International SAMPE Symposium* (2003), 261-264
9. **Yamamoto, T.**, **Takeda, S.**, **Okabe, Y.** and **Takeda, N.**, "Health monitoring of a bonded repair patch using small-diameter FBG sensors", *Proc. 8th Japan International SAMPE Symposium* (2003), 159-162